Structural Investigation of MFe_2O_4 (M = Fe, Co) Magnetic Fluids

Guilherme V. M. Jacintho,[†] Alexandre G. Brolo,[‡] Paola Corio,[§] Paulo A. Z. Suarez,[†] and Joel C. Rubim*[,†]

Laboratório de Materiais e Combustíveis (LMC), Instituto de Química da Universidade de Brasília, CP 04478, 70919-970, Brasília, DF, Brazil, Department of Chemistry, University of Victoria, P.O. Box 3065, Victoria, British Columbia, Canada, V8W 3V6, Instituto de Química da Universidade de São Paulo, CP 26.077, 05513-970, São Paulo, SP, Brazil

Received: February 13, 2009; Revised Manuscript Received: March 19, 2009

Ferrites of the type $M^{II}Fe_2O_4$ (M = Fe and Co) have been prepared by the traditional coprecipitation method. These ferrites were modified by the adsorption of fatty acids derived from soybean and castor oil and were then dispersed in cyclohexane, providing very stable magnetic fluids, readily usable in nonpolar media. The structural properties of the ferrites and modified ferrites as well as the magnetic fluids were characterized by XRD (X-ray powder diffraction), TEM (transmission electron microscopy), DRIFTS (diffusion reflectance infrared Fourier transform spectroscopy), FTNIR (Fourier transform near-infrared), UV−vis, normal Raman spectroscopy, and surface-enhanced Raman scattering (SERS). XRD and TEM analysis have shown that the magnetic nanoparticles (nonmodified and modified) present diameters in the range of 10−15 nm. DRIFTS measurements have shown that the carboxylate groups of soybean and castor oil fatty acids adsorb on the ferrite surface, forming three different structures: a bridging bidentate, a bridging monodentate, and a bidentate chelate structure. The FTIR and Raman spectra of nonmodified Fe_3O_4 and $CoFe_2O_4$ nanoparticles have shown that the number of observed phonons is not compatible with the expected O_h^7 symmetry, since IR-only active phonons were observed in the Raman spectra and vice versa. SERS measurements of a $CoFe_2O_4$ thin film on a SERS-active gold electrode at different applied potentials made possible the assignment of the signals near 550 and 630 cm^{-1} to Co−O motions and the signals near 470 and 680 cm^{-1} to Fe−O motions.

Introduction

The earliest reports on the synthesis of magnetic iron oxide particles forming relatively stable colloids date from the decade of 1930.[1,2] However, the first stable suspension of magnetic particles was only obtained by Papell[3] almost 30 years after the first reports. Papell's magnetic fluid (MF) was a dispersion of magnetite (Fe_3O_4) particles (diameter <25 μm) modified by oleic acid. These particles were dispersed in nonpolar solvents (carrier), forming a stable MF that was used to confer magnetic properties to fuels. After that, Rosensweig[4,5] obtained several kinds of MFs with different carrier solvents, such as kerosene, water, fluorocarbons, and esters. It is worth mentioning that all these MFs were obtained by the dispersion of ground magnetite particles.

In 1979, Massart[6] dispersed magnetite nanoparticles without surfactants in polar solvents. These MFs were obtained by a chemical procedure involving the coprecipitation of Fe(II) and Fe(III) hydroxides. Later, Tourinho et al.[7,8] modified Massart's process and were able to obtain ultrastable and highly concentrated MFs with different magnetic particles based on spinel ferrites such as $[(M_{1-x}^{2+}Fe_x^{3+}]_A[Fe_{2-x}^{3+}M_x^{2+}]_BO_4$ (M = Mn, Co, Ni, Cu, and Zn).

Magnetic fluids present applications in different fields, such as diagnosis of diseases, targeted drug delivery, hyperthermia, magnetic resonance imaging, sensors, actuators, magnetic storage devices, etc. (for a recent review on these applications see ref 9). For biomedical applications, the particles have their surface modified to be stable at physiological pH as well as at the blood ionic strength. In general, biocompatible MFs are obtained by surface modification with dicarboxylic acids[10,11] or carboxydextran.[12] On the other hand, MFs used in chemical sensors, actuators, and micro-/nanofluidic device applications require that the nanoparticles be stable in carriers of different polarity, including nonpolar organic solvents such as hexadecane.[13] For stabilization in nonpolar solvents, the nanoparticles should have their surface modified by the adsorption of long-chain carboxylic acids, such as oleic acid,[5,13] and the process initially involves the synthesis of the magnetic nanoparticles, followed by their surface modification with a fatty acid.

There are several reports in the literature with regard to the synthesis of magnetic nanoparticles dispersible in nonpolar solvents. These methods have been recently reviewed.[9] In general, these methods involve the sonochemical or thermal decomposition of precursors such as $FeCup_3$ (Cup: *N*-nitrosophenylhydroxylamine),[14] $Fe(CO)_5$,[15,16] ferric triacetylacetonate ($Fe(acac)_3$) or $2Fe(acac)_3/1M(acac)_2$ mixtures for the synthesis of MFe_2O_4 (M = Co, Mn) nanocrysltals,[17] and $Fe(oleate)_3$[18,19] in the presence of oleic acid, oleylamine, and cosurfactants. Recently, Wang et al.[20] obtained γ-Fe_2O_3 nanocrystals by the decomposition of $Fe(CO)_5$, followed by oxidation, in the presence of oleylamine and oleic acid at 280 °C using an ionic liquid, 1-*n*-butyl-3-methylimidazolium trifluoromethanosulfoimide ($BMITf_2N$), as a solvent.

Bulk magnetite (Fe_3O_4) and $CoFe_2O_4$ are reported as having an inverse spinel cubic structure belonging to the O_h^7 ($Fd\bar{3}m$) space group.[21−23] Although their X-ray powder diffraction patterns are quite similar,[24] their Raman spectra are quite

* To whom correspondence should be addressed. E-mail: jocrubim@unb.br.
† Instituto de Química da Universidade de Brasília.
‡ University of Victoria.
§ Instituto de Química da Universidade de São Paulo.

10.1021/jp9013477 CCC: $40.75
Published on Web 04/13/2009

different. For the cubic symmetry, one expects the following optical phonon distribution: $5T_{1u} + A_{1g} + E_g + 3T_{2g}$; the $5T_{1u}$ modes are IR active,[25] whereas the other five modes are Raman-active.[21,23,25,26] Chourpa et al.[27] have observed a large number of features in the Raman spectrum of magnetite nanoparticles that are not compatible with the bulk cubic symmetry. Similar observations have been reported for $CoFe_2O_4$ nanoparticles.[22,28,29] As will be shown in the present work, we also observe Raman spectra for Fe_3O_4 and $CoFe_2O_4$ nanoparticles with more Raman bands than expected for cubic symmetry. Therefore, it seems that the structure of nanoparticles of these materials is very different from the bulk and deserves further investigation.

In this sense, the present work aims at the investigation of the nanostructure of Fe_3O_4 and $CoFe_2O_4$ nanoparticles by X-ray powder diffraction (XRD), FTNIR, FTIR, Raman, and surface enhanced Raman scattering (SERS). The most relevant ferrite nanoparticles in terms of applications are capped with long-chain fatty acids. In our investigations, the ferrite surfaces were modified by fatty acids of raw vegetable oils, such as soybean and castor oil. It is worth mentioning that most of the methods for the synthesis of ferrites described in the literature used complex precursors. Furthermore, in those methods, the modification of the nanoparticle surface requires the use of expensive and complex surfactants, whereas in the method proposed in this work, readily accessible renewable resources (raw vegetable oils) were used.

Experimental Part

Reagents. $FeCl_3 \cdot 6H_2O$ 97% (from LabSynth LTDA), $CoCl_2 \cdot 6H_2O$ 98%, $FeSO_4 \cdot 7H_2O$ 99%, NH_4OH 28%, and acetone 99.5%, HCl, NaCl, Na_2SO_4, and $MgSO_4$ were analytical grade reactants from VETEC Química Fina LTDA and were used as received. The refined soybean oil was obtained from Bunge (Luziania, GO, Brazil), and the crude castor oil was obtained from A. Azevedo Ind. e Com. de Óleos LTDA (SP, Brazil).

Preparation of Carboxylic Acid Mixtures from Soybean and Castor Oils. Both vegetable oils were used as received without further purification and were treated according to the following procedure: First, the oil was submitted to a saponification reaction with NaOH. The glycerin formed was removed by washing the soap with a saturated aqueous NaCl solution. The fatty acid salt was then dissolved in water and acidified with a 3 mol L^{-1} HCl solution under vigorous stirring. A homogeneous emulsion of fatty acids in water was formed after the acidification process. The emulsion was then heated to promote its separation from water. The fatty acids were dissolved in dichloromethane, and the residual water was removed with anhydrous sodium and magnesium sulfates. After filtering the mixture, the solvent was removed in a rotary evaporator, and a pale-yellow mixture of fatty acids was obtained.

The content of fatty acids in the soybean oil was determined in a Shimadzu LC-20AT HPLC instrument equipped with a reversed-phase column (Shim-pack VP-ODS, particle size 4.7 μm, 250 × 4.6 mm i.d. from Shimadzu). All solvents were of HPLC grade and were used without further purification. Fatty acids were separated in 25 min using a combined linear gradient with aqueous−organic and nonaqueous mobile phase steps: 70% acetonitrile + 30% water for 0 min, 100% acetonitrile for 10 min, 50% acetonitrile + 50% 2-propanol/hexane (5:4, v/v) for 20, and 5 min final hold-up. The major constituents of soybean oil as determined by HPLC are linoleic (56% w/w, C18:2, 9(*Z*),12(*Z*)-octadecenoic acid) and oleic (23% w/w, C18:1, 9(*Z*)-octadecanoic acid) fatty acids, which is the expected composition for this kind of vegetable oil.[30]

The fatty acids mixture obtained from castor oil was first converted to its methyl ester derivatives by an esterification reaction. Ten milliliters of the fatty acid mixture, 150 mL of MeOH, and 10 mL of concentrated H_2SO_4 were maintained under reflux for 3 h. The organic phase (the methyl esters) was extracted with CH_2Cl_2, and its excess was removed by vacuum evaporation. The methyl esters were then analyzed by gas chromatography on a Shimadzu GC-17A chromatograph equipped with a FID detector and using a polydimethylsiloxane column (CBPI PONA-M50-042, 30 m, 0.25 mm i.d., and film thickness of 0.2 μm) at temperatures varying from 80 to 250 °C, with a heating rate of 10 °C/min. The major constituent of the castor oil as determined by GC is the ricinoleic acid (97% w/w, C18:1,12:OH, 12-hydroxy-9(*Z*)-octadecenoic acid).

Synthesis of MFe_2O_4 (M = Fe, Co). Magnetite (Fe_3O_4) nanoparticles were obtained by the coprecipitation method[7,8] by adding a deaereated acid solution of $FeSO_4$ (0.09 mol L^{-1}) and $FeCl_3$ (0.18 mol L^{-1}) to a deaerated solution of NH_4OH (1.5 mol L^{-1}) at 60 °C under vigorous stirring. Cobalt ferrite was prepared by adding 120 mL of NaOH (2 mol L^{-1}) to 500 mL of an acid solution of $FeCl_3$ (0.05 mol L^{-1}) and $CoCl_2$ (0.025 mol.L^{-1}) at 95 °C and under vigorous stirring.[31]

Synthesis of MFe_2O_4 (M = Fe, Co) Modified by Fatty Acids. Three types of modified ferrites were prepared: (i) Fe_3O_4 modified by carboxylic acids derived from soybean oil (Fe_3O_4/SO), (ii) Fe_3O_4 modified by carboxylic acids from castor oil (Fe_3O_4/CO), and (iii) $CoFe_2O_4$ modified by soybean oil carboxylic acids ($CoFe_2O_4$/SO). The functionalization of ferrites was carried out as follows: The black precipitate obtained just after the ferrite synthesis was washed with water until pH 8 was reached. The ferrite was kept in distilled water at 95 °C, and the carboxylic acid mixture was slowly poured into the suspension under mild mechanic stirring. At the end of the fatty acid addition, the material coagulated and was easily removed from the supernatant. The coagulated material was then washed with acetone to remove the free fatty acids. The functionalized nanoparticles were separated from the acetone by decantation with the help of a magnet. The obtained precipitate was readily dispersed in cyclohexane or toluene, forming a stable nonpolar MF.

Instrumentation. The XRD patterns were obtained on a XRD instrument from Rigaku Geigerflex model D/MAX-2AC. The excitation wavelength was 1.540 562 Å. Transmission electron microscopy (TEM) images were obtained on a Hitachi H-7000 transmission electron microscope.

The diffusion reflectance infrared Fourier transform (DRIFT) and transmission FTIR spectra were obtained on an Equinox 55 (Bruker). Each DRIFT or FTIR spectrum is the average of 32 scans (interferograms) at 4 cm^{-1} nominal resolution. The FTIR transmission spectra were obtained from sample liquid films using NaCl windows. The DRIFT spectra were obtained using a DRIFT accessory from Harrick. The FTNIR transmission spectra from liquid samples were obtained on the Equinox 55 equipped with a Ge detector. Each FTNIR spectrum is the result of 16 scans at 8 cm^{-1} nominal resolution and was obtained from liquid films using NaCl windows. The Raman spectra, excited at 632.8 nm (Spectra Physics), were obtained in the backscattering geometry using a Renishaw Raman System 3000 equipped with an Olympus microscope with a 50× objective. The spectral resolution was 6 cm^{-1}. The laser power when

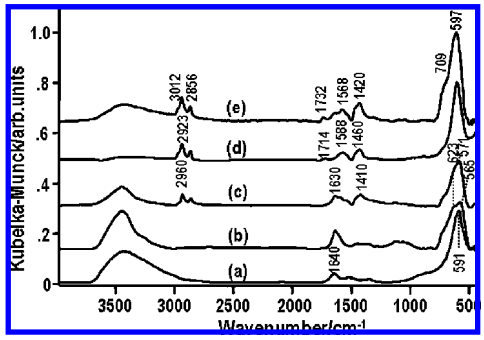

Figure 1. DRIFT spectra of (a) $CoFe_2O_4$, (b) Fe_3O_4, (c) Fe_3O_4/CO, (d) $CoFe_2O_4$/SO, and (e) Fe_3O_4/SO.

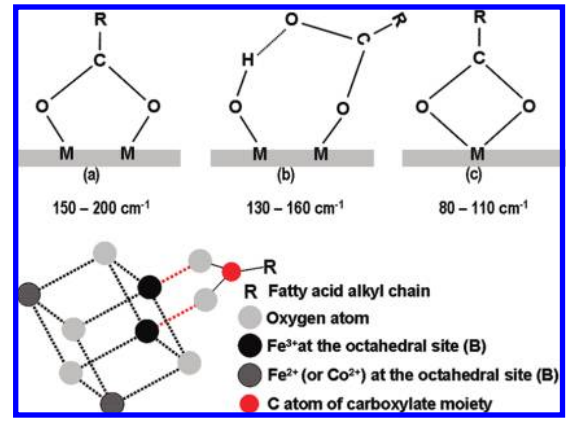

Figure 2. Schematic pictures representing the three types of coordination of the carboxylate group to the nanoparticles and an illustration of carboxylate bonding to Fe^{3+} ions at an octahedral site of an inverse spinel, forming a bridging bidentate structure. See text for details.

measuring the samples as powders was ~0.2 mW at the sample to avoid their degradation.

SERS Measurements. The electrode used in the SERS measurements was a gold rod (99.999%) with 0.2 cm^2 of geometrical area inserted in polytetrafluorethylene. A Pt wire was used as an auxiliary electrode, and all potentials are referred to an Ag/AgCl reference electrode. The electrochemical system used in the SERS measurements was an EG&G PAR 263 potentiostat/galvanostat. The Au electrode was activated in NaCl 0.1 mol L^{-1} solution following the procedure described by Liu et al.[32] After that, the electrode was washed with doubly distilled water, dried in air, and then exposed to a drop of a colloidal water solution of $CoFe_2O_4$ nanoparticles for 60 s. Then the electrode was thoroughly washed with doubly distilled water, followed by ethanol; dried in the air; and then transferred to the spectroelectrochemical cell for the SERS measurements.

3. Results and Discussion

3.1. Structure of the Adsorbed Fatty Acids. The ferrite nanoparticles, nonmodified and modified by the adsorption of carboxylic acids, presented mean diameters in the 10−15 nm range as determined by XRD and TEM measurements. To evaluate how these carboxylic acids interact with the ferrite nanoparticles, DRIFT spectra were recorded. The DRIFT spectra of the Fe_3O_4, $CoFe_2O_3$, Fe_3O_4/SO, Fe_3O_4/CO, and $CoFe_2O_3$/SO samples are displayed in Figure 1. The infrared transitions labeled in Figure 1, as well as those observed in the FTIR spectra of the soybean and castor oil fatty acids, are displayed in Table 1 with the corresponding tentative assignment.

Infrared spectroscopy has been used to investigate the structure of long chain carboxylic acids adsorbed on oxide−metal[33−35] and metal surfaces.[36−38] In general, the carboxylate moiety interacts directly with these surfaces, following Nakamoto's proposed structures for metal−carboxylate compounds.[39] According to Nakamoto, the difference (Δ) in wavenumbers between the asymmetric (ν_{as}(COO)) and symmetric (ν_s(COO)) stretching modes of the carboxylate group can be used to determine the interaction type between the carboxylate head and the surface metal ion. Figure 2 shows schematic pictures of the possible adsorption models according to the values of Δ. The bridging bidentate structure (Figure 2a) corresponds to Δ values ranging from 150 to 200 cm^{-1}. The bridging monodentate (Figure 2b) and the bidentate quelate (Figure 2c) structures are for Δ values ranging from 130 to 160 cm^{-1} and from 80 to 110 cm^{-1}, respectively.

The observed wavenumbers associated with the ν_{as}(COO) and ν_s(COO) vibrational modes for the investigated modified ferrites and the corresponding Δ (ν_{as}(COO)−ν_s(COO)) values are displayed in Table 2. Three bands assignable to ν_{as}(COO) were observed for each ferrite (Table 1), which indicates a distribution of adsorption geometries. In fact, the Δ values (Table 2) show the carboxylate groups interacting with the metal ions on the magnetic nanoparticles through the three types of coordination. It is worth mentioning that the absorptions centered at 1522/1524 cm^{-1} (ν_{as}(COO)) present lower intensities when compared to the absorptions at 1600/1588 cm^{-1} and 1568/1545 cm^{-1}. This may indicate that the surface concentration of the bidentate structure (Figure 2c) is smaller than the other two.

TABLE 1: Main Infrared Transitions Observed in the FTIR Spectra of the Vegetable Oils and in the DRIFT Spectra of the Fatty Acid-Modified Ferrites[a]

soybean oil	castor oil	Fe_3O_4/CO	$CoFe_2O_4$/SO	Fe_3O_4/SO	assignment
	3390 (br)	3421 (vbr)	3405 (mw, br)	3440 (vbr)	ν(OH)
3012 (m)	3011 (w)	3012	3010 (w)		ν(=C−H)
2960 (sh)	2960 (sh)	2960 (sh)	2960 (sh)	2960 (sh)	$\nu_a(CH_3)$
2923 (VS)	2927 (vs)	2923 (m)	2923 (m)	2923 (m)	$\nu_a(CH_2)$
2856 (s)	2856 (s)	2856 (mw)	2856 (mw)	2856 (mw)	ν_s(CH)
		1732 (w)	1739 (sh)		ν(C=O)
1711 (vs)	1711 (s)	1714 (vw)	1714 (w)		ν(C=O)
	1626 (w)	1629 (br)	1631 (br)	1620 (m)	δ(OH)
		1600 (sh)	1588 (m)	1580 (sh)	ν_{as}(COO)
		1568 (m, br)	1545 (mw)		ν_{as}(COO)
		1524 (w, sh)	1522 (sh)	1524 (sh)	ν_{as}(COO)
1462 (m)	1462 (m)	1460 (sh)	1464 (sh)	1460 (sh)	$\delta(CH_2)$
1435 (m)	1435 (m)		1438 (m)		
1413 (m)	1413 (m)	1420 (m)	1413 (m)	1410 (m)	ν_s(COO)

[a] sh, shoulder; w, weak; m, medium; s, stronger; vs, very strong; br, broad.

TABLE 2: The ν_{as}(COO) and ν_s(COO) Wavenumbers Observed in the DRIFT Spectra of the Investigated Fatty Acid-Modified Ferrites, Corresponding Δ Values, and Coordination Types

assignment	Fe_3O_4/SO	Δ (cm^{-1})	Fe_3O_4/CO	Δ (cm^{-1})	$CoFe_2O_4$/SO	Δ (cm^{-1})	coordination type
ν_{as}(COO)	1580 (sh)	170	1600 (sh)	180	1588 (m)	175	Figure 2a, bridging bidentate
ν_{as}(COO)			1568 (m, br)	148	1545 (mw)	132	Figure 2b, bridging monodentate
ν_{as}(COO)	1524 (sh)	114	1524 (w, sh)	104	1522 (sh)	99	Figure 2c, bidentate quelate
ν_s(COO)	1410 (m)		1420 (m)		1413 (m)		

TABLE 3: IR and Raman Phonons of Fe_3O_4 Samples and Corresponding Assignment[a]

Fe_3O_4[21,26]	Fe_3O_4[41]	Fe_3O_4[b]	Fe_3O_4/SO[b]	Fe_3O_4/CO[b]	assignment[26,41]
193	193	179	184	178	t_{2g}
(210)[c]					t_{1u}
(270)		270	270	273	t_{1u}
308	306	315	313	315	e_g
(350)					t_{1u}
		374	373	375	γ-Fe_2O_3
	450−490	445	448	435	t_{2g}
		501	502	502	γ-Fe_2O_3
540	538	(530)	(535)	(537)	t_{2g}
(560)		565 (565)	559 (571)	554 (559)	t_{1u}
		627 (624)	621 (623)	619 (625)	γ-Fe_2O_3
670	668	664 (667)	666 (670)	665 (660)	a_{1g}
		712 (712)	715 (714)	711 (709)	Fe(III)[d]

[a] For comparison, results from the literature (from bulk) are also presented. [b] This work. [c] Values in parentheses are IR data. [d] Oxidation of Fe(II) centers at octahedral sites.

3.2. Analysis of Infrared and Raman Phonon Modes of Magnetite. The unit cell of magnetite contains 56 atoms and at room temperature has a cubic inverse-spinel structure that belongs to the O_h^7 ($Fd\bar{3}m$) space group. The smallest Bravais cell contains only 14 atoms, and 42 vibrational modes are expected. There are $5t_{1u}$ phonon modes that are IR-active and another 5 phonon modes ($a_{1g} + e_g + 3t_{2g}$) that are Raman-active.[21] For the single crystalline bulk magnetite at temperatures above the Verwey transition (T_v = 121 K), only two phonons are observed in the mid-IR region at 350 and 560 cm^{-1}.[21] The 560 cm^{-1} band has a full width at half-maximum (fwhm) value of ~50 cm^{-1}.[21] At temperatures below the Verwey transition, this absorption shifts to higher wavenumbers and broadens (fwhm ~80 cm^{-1}).[21] It is well-known that at the Verwey transition, the magnetite crystal has its symmetry reduced to orthorhombic,[21,40] and this change in the crystal structure explains the broadening of IR absorptions as well as their shift in wavenumber position.

The IR spectra of magnetite and modified magnetite nanoparticles show a strong absorption near 570 cm^{-1} that is assigned to the t_{1u} phonon involving Fe−O bonds. However, we have observed that the infrared absorption near this wavenumber presents some additional features as the shoulders near 620 and 705 cm^{-1} (see Figure 1). We have then performed a curve-fitting analysis of these absorptions, and the obtained results are displayed in Table 3.

Table 3 shows that the number of observed IR phonon absorptions in the 500−750 cm^{-1} region for the nanoparticles is larger than expected for a regular cubic symmetry of the bulk. These results were confirmed by Raman scattering. The Raman spectra of nonmodified and fatty acid-modified magnetite nanoparticle samples are displayed in Figure 3a−c. Some of the Raman signals displayed in Figure 3 are very broad, suggesting that they may be composed of more than one Raman band. The Raman spectra of these samples were also curve-fitted to isolate these contributions. The corresponding results are also displayed in Table 3. Note that even without the curve-fitting analysis, it is possible to note from Figure 3 that the number of observed Raman phonons is not consistent with a cubic symmetry.

Maghemite presents an IR absorption at 620 cm^{-1} [42] and broad Raman phonons near 370 and 500 cm^{-1}.[43,44] Therefore, a possible explanation for the observation of the IR absorption near 624 cm^{-1} and the broad Raman features near 500 and 376 cm^{-1} can be the partial oxidation of magnetite to maghemite. The shoulder observed near 710 cm^{-1} in the IR and Raman spectra of magnetite samples (see Figures 1 and 3) is attributed to the oxidation of Fe(II) centers (in octahedral sites) to Fe(III), leading to the formation of a nonstoichiometric Fe(III) oxyhydroxide.[45] The presence of such a species on the surface of magnetite could explain the observation of Δ values corresponding to the formation of bridging monodentate structures (see Figure 2 and Table 2). It is worth mentioning that the intensities of the phonons corresponding to the presence of oxidized species such as γ-Fe_2O_3 are higher for the Fe_3O_4 and Fe_3O_4/SO samples than for the Fe_3O_4/CO sample. The latter was prepared just after the synthesis of magnetite, whereas the Fe_3O_4/SO sample was prepared 6 h after the synthesis of the magnetite. Partial oxidation of the samples was expected, since the IR and Raman spectra were recorded in the air. The oxidation of Fe(II) to Fe(III) in magnetite was also observed by Chourpa et al.[27]

As mentioned above, at room temperature, bulk magnetite (Fe_3O_4) belongs to the O_h^7 space group, and five Raman optical phonons are expected ($a_{1g} + e_g + 3t_{2g}$).[21,26,40,41] Shebanova and Lazor[41] have performed Raman polarization measurements on a Fe_3O_4 single crystal and have characterized the Raman phonons of magnetite, including the e_g mode at 306 cm^{-1}. Therefore, the assignment of the Raman phonons as presented in Table 3 follows Shebanova and Lazor work. The results of Table 3 show that at least 10 phonons were observed in the Raman spectrum of magnetite nanoparticles. Even if we remove the contributions from oxidized species, we still have seven phonons remaining that represent an unexpected number of phonons for the cubic symmetry assumed for magnetite. It is worth mentioning that phonons that are expected to be IR-active appeared in the Raman spectra and vice versa, such as the t_{1u} phonons near 270 and 560 cm^{-1}, observed in the Raman and

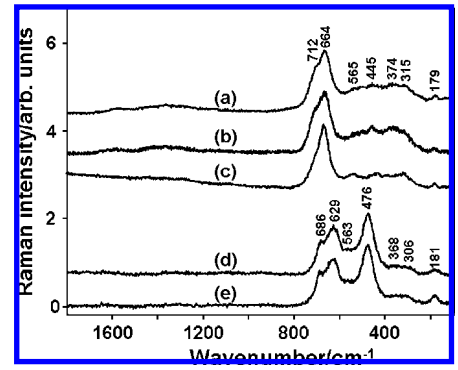

Figure 3. Raman spectra excited at 632.8 nm of (a) Fe_3O_4, (b) Fe_3O_4/SO, (c) Fe_3O_4/CO, (d) $CoFe_3O_4$, and (e) $CoFe_3O_4$/SO.

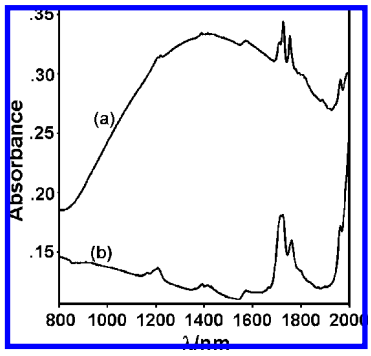

Figure 4. FTNIR spectra of films of Fe_3O_4/SO dispersed in cyclohexane and (b) soybean fatty acids.

the a_{1g} phonon that was observed in the IR spectra. Therefore, the selection rules for the cubic symmetry of the magnetite nanoparticle samples have been broken. Since the measurements were performed at room temperature, a reduction in the symmetry due to the Verwey transition cannot account for these observations.

To explain the above results, we propose a breakdown of the momentum conservation rule, since the wavelength of the exciting radiation (632.8 nm) is much larger than the particle diameter (~10 nm). The wavevector (k) for a finite particle of size L is given by the expression $k = \pm(2\pi)/(L)$, and the observed Raman signals should follow the phonon dispersion at $k = \pm(2\pi)/(L)$. In the case of a crystal with L much larger than the wavelength, that is, $k = 0$, it means that only the zone center phonons are allowed in the Raman scattering due to the momentum conservation rule. However, if L is much smaller than L, the momentum conservation rule breakdown and phonons for $k \neq 0$ become allowed. For instance, inactive Raman phonons at $k = 0$ become active at $k \neq 0$ for graphite microcrystallites[46] or carbon nanohorns.[47] In the case of magnetite, the O_h^7 symmetry defines the number of active Raman phonons for $k = 0$. However, for $k \neq 0$, the symmetry is no longer the same, and other phonons become Raman-active. Hanke et al. have performed an ab initio calculation for the phonon dispersion of magnetite (see Figure 8 in ref 48). At the Γ center, the number of phonons is those expected for the cubic symmetry, but as the wavevector departs from the Γ center, there is a considerable increase in the number of phonons. Therefore, we believe that for $k \neq 0$, the inversion center of the cubic centrosymmetric crystal is absent, which explains the observation of IR phonons in the Raman spectra and vice versa.

One could argue that the nanoparticle samples are maghemite rather than magnetite. However, magnetite presents a very broad absorption in the near-infrared (NIR) region and maghemite does not.[49−51] Figure 4 shows the FTNIR spectra of the Fe_3O_4/SO sample and that of the soybean fatty acids for comparison. Note that the FTNIR spectrum of Fe_3O_4/SO presents a broad absorption centered at ~1400 nm. As demonstrated in refs 45 and 51, maghemite does not absorb in this spectral region.

3.3. Analysis of the IR and Raman Phonon Modes of $CoFe_2O_4$. The reported IR spectra of $CoFe_2O_4$ nanoparticles prepared according to different procedures usually show two absorption bands, at 389 cm^{-1} [52,53] and ~586−590 cm^{-1}.[52−56] The DRIFT spectra of nonmodified and modified $CoFe_2O_4$ nanoparticle samples (Figure 1) present a very strong absorption centered at 591 cm^{-1}. However, by expanding this spectral region and performing a curve-fitting procedure, other absorptions were identified and are displayed in Table 4. The strongest absorption peak is the one centered at 591 cm^{-1} that is assigned to a t_{1u} phonon in an O_h^7 environment. In comparison to magnetite, the other t_{1u} phonons are expected to appear bellow 400 cm^{-1}; however, our IR spectra do not cover this spectral region; neither is there a work in the literature reporting the IR spectrum of a $CoFe_2O_4$ covering the region below 350 cm^{-1}. The absorption features extracted from the curve-fitting analysis suggest that the $CoFe_2O_4$ nanoparticles have structures different from that of a spinel cubic structure.

TABLE 4: IR and Raman Phonons of $CoFe_2O_4$ Nanoparticles and Corresponding Assignment[a]

$CoFe_2O_4$[23]	$CoFe_2O_4$[57]	$CoFe_2O_4$[28]	$CoFe_2O_4$[b]	$CoFe_2O_4$/SO[b]
785 nm	514.5 nm	532 nm		
188	190	180	181	179
300	300	308	306	305
	340	360	368	364 389[c]
			439	437
471	475	475	476	475
	516		524	525
563			563 (556)[d]	564 (553)
		580	(588)	(591)
617	610	630	629 (630)	629 (629)
683	680	690	686 (679)	687 (680)
			714 (714)	716 (715)

[a] For comparison, results from the literature are also presented. [b] This work. [c] IR absorption observed in refs 52 and 53. [d] Values in parentheses are IR absorptions.

A similar behavior was observed in the Raman spectra of the $CoFe_2O_4$ samples (see Figure 3d, e). Note that the indicated Raman features, seven, is larger than the five expected for a cubic symmetry. Other features were obtained after a curve-fitting analysis and are presented in Table 4.

In the case of the $CoFe_2O_4$ ferrites, we found some controversy regarding the crystal structure, as well as in relation to the features observed in the Raman spectra. For instance, Wang et al. have synthesized bulk $CoFe_2O_4$ ferrites and characterized the 0.1 mm crystals by X-ray diffraction and Raman spectroscopy at different pressures.[23] According to these authors, their $CoFe_2O_4$ sample has a tetragonal structure and belongs to the $I4_1/amd$ space group ($Z = 8$). It is worth mentioning that the number of phonons observed in Figure 3d, e is larger than those reported in ref 23, but the relative intensities observed in Figure 3d, e are quite similar to those observed by Wang et al.[23] On the other hand, some research groups[22,28,29,57−61] have recorded Raman spectra of $CoFe_2O_4$ samples and interpreted them as the Coferrites presenting a cubic-inverse spinel structure belonging to the O_h^7 ($Fd\bar{3}m$) space group. As mentioned above, for this symmetry, one expects five Raman-active phonons ($a_{1g} + e_g + 3t_{2g}$). However, the spectra reported in refs 22, 28, 29, 57, and 61 present a number of Raman features that are not compatible with this symmetry, since at least six to seven Raman features are observed in these reports (some of them are displayed in Table 4). It is worth mentioning that the Raman spectrum of a $CoFe_2O_4$ reported in Figure 4 of ref 22 shows Raman features near 310, 370, 470, 560, 620, and 680 cm^{-1} in addition to an asymmetry to wavenumbers above 680 cm^{-1} that suggests a shoulder near 710 cm^{-1}. Furthermore, the region below 300 cm^{-1} was not shown, and therefore, nothing can be said regarding the absence or presence of the Raman feature near 180 cm^{-1}.

The IR absorption near 715 cm^{-1} (see Table 4) was also observed as a shoulder in the IR spectra of $CoFe_2O_4$ samples reported by Tirosh et al.[55] and Calero-DdelC and Rinaldi.[56] Tirosh et al. assigned this feature to Co_3O_4;[55] however, this feature does also appear in the Raman spectra of Coferrite and

magnetite samples. As in the case of magnetite, we assign this feature to the formation of a nonstoichiometric Fe(III) oxyhydrodroxide,[45] even though the number of Raman and IR phonons reported in Table 4 for the investigated $CoFe_2O_4$ samples are still too large for an O_h^7 symmetry.

If we consider that the $CoFe_2O_4$ nanoparticles have their octahedral structure distorted as the one obtained by Wang et al.,[23] then a tetragonal structure could be the answer for the number of observed phonons. Factor group analysis yields 10 active Raman modes ($2a_{1g} + 3b_{1g} + b_{2g} + 4b_g$) for tetragonal $CoFe_2O_4$.[23] It is worth mentioning that the tetragonal structure obtained by Wang et al. was achieved after heating the sample for 20 h at 1050 °C.[23] However, as shown in Table 4, there are at least three Raman features that are also observed in the IR spectra. Therefore, we believe that the results cannot be explained by simple symmetry-breaking. We then assign this discrepancy to quantum size effects. Since the size of the nanoparticles is much smaller than the laser wavelength, the momentum conservation rule is broken, and phonons for $k \neq 0$ become allowed.

Another interesting aspect in the Raman spectra of $CoFe_2O_4$ nanoparticles is the relative intensity of the phonons observed near 474, 620, and 680 cm^{-1}. The feature at 680 cm^{-1} appears as the most intense in the majority of the spectra excited at laser wavelengths bellow 540 nm,[28,29,57] whereas in the Raman spectra excited at 785 nm[23] or those reported here (at 632.8 nm excitation), the highest intensity is observed for the Raman feature near 474 cm^{-1}. However, in the work of Shemer et al.,[22] the Raman spectra of $CoFe_2O_4$ samples were excited at 632.8 nm, and they observed relative intensities different from those reported in the present work. For instance, although for sample V (see Figure 3A of ref 22) the intensity of the feature near 474 cm^{-1} is higher than that of the signal near 680 cm^{-1}, the opposite was observed for sample IV (see Figure 3B of ref 22). According to these authors, the changes in the relative Raman intensities from sample to sample would be due to differences in Co^{2+} incorporation into the lattice since they assigned the Raman signal at 474 cm^{-1} to a vibrational mode involving Co^{2+} at octahedral sites and the Raman signal near 680 cm^{-1} was assigned to a vibrational mode with contributions from magnetite and Coferrite phases in the nanoparticles.[22]

With regard to the differences in the relative intensities mentioned above, there are some considerations to be made. The structure of $CoFe_2O_4$ is that of a $B(AB)O_4$ inverse spinel with half of the Fe^{3+} cations occupying tetrahedral sites (B) and the other half of Fe^{3+} ions and the Co^{2+} ions occupying the octahedral sites (AB).[62] It is well-known that the temperature has a significant effect on the Co^{2+} distribution in the lattice of the spinel structure.[62] The Raman spectra reported in refs 28, 29, and 58 correspond to samples that have been calcinated or annealed at very high temperatures (above 1000 °C). The Raman spectra were excited at 514.5 or 488.0 nm, and in all spectra, the intensity of the signal near 680 cm^{-1} was higher than the one near 470 cm^{-1}.[28,29,58] On the other hand, the $CoFe_2O_4$ sample reported as tetragonal was annealed at 1050 °C,[23] but its Raman spectrum, excited at 745 nm, shows relative intensities similar to those reported in the present work, where the 474 cm^{-1} feature appears as the strongest signal. Therefore, it seems that the differences on the relative intensities reported in the literature are dependent on the laser excitation wavelength and not on the temperature used in the sample preparation. To verify if the laser excitation would affect the relative intensities, we have recorded the Raman spectra of the $CoFe_2O_4$ (nonmodified by fatty acids) at 514.5 and 647.1 nm using Na_2SO_4 as an internal standard for intensity normalization. The spectra were recorded from a solid solution of $CoFe_2O_4$ and Na_2SO_4, and the results are displayed in Figure 5. It is worth mentioning that a spinning cell was used to avoid sample heating. Note that the intensity of the signal at 686 cm^{-1} in the spectrum excited at 647.1 nm is nearly half that of the signal at 475 cm^{-1}, but at 514.5 nm excitation, these features have almost the same intensity. This is an indication that some resonance process involving ground and excited electronic states in Coferrite is operating. Shemer et al. have observed that on the Stokes side of the Raman spectrum of a $CoFe_2O_4$ sample, the 475 cm^{-1} signal is stronger than the one near 680 cm^{-1}, and that on the anti-Stokes side, the 680 cm^{-1} feature was stronger than the 475 cm^{-1}.[22] They have proposed that this difference in the relative intensities would be due to a resonance process.

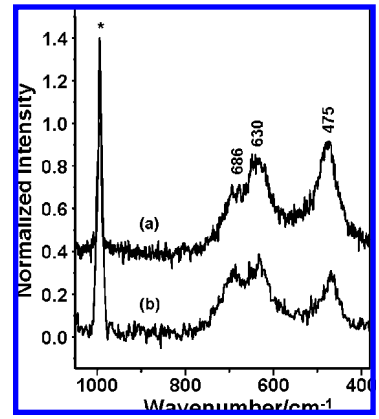

Figure 5. Raman spectra of $CoFe_2O_4$ nanoparticles excited at 647.1 (a) and 514.5 nm (b). The asterisk is the Raman signal of Na_2SO_4 that was used as an internal standard for intensity normalization.

It is worth mentioning that Qu and co-workers have recorded the Raman spectra of $CoFe_2O_4$ excited at 514.5 nm.[63] Their Coferrite samples were prepared using a procedure similar to the one reported in this work, and their samples were exposed to temperatures not higher than 100 °C. Their Raman spectra show that the observed Raman features are all shifted ~20 cm^{-1} to lower wavenumbers, probably due to a spectrometer calibration problem. However, the relative intensities of the features corresponding to the signals at 686 and 474 cm^{-1} are very close to those shown in Figure 5b. Therefore, the small discrepancies between the relative intensities in the Raman spectra of $CoFe_2O_4$ excited at 632.8 nm as reported by Shemer et al.[22] relative to those presented here may be due to the fact that they have used higher temperatures, ~300 °C, in their synthesis, as compared to the temperature synthesis of the present work (95 °C).

Another question to be addressed is, which observed Raman phonons have contribution from Co−O motion? The results of Figure 5 show that the Raman phonon near 630 cm^{-1} does also present relative intensities that change with the laser excitation. Therefore, it is difficult to address this question only on the basis of the Raman spectra. Jacintho et al. have demonstrated that the use of SERS on electrode surfaces made possible the assignment of the observed Raman phonons of maghemite nanoparticles to the different chemical species composing that nanostructured material.[45] The results of Figure 6 show SERS spectra at different electrode potentials of a thin film of $CoFe_2O_4$ deposited on a previously activated Au electrode. The remarkable result is the fact that the SERS features at 629 and 553 cm^{-1}, which are very well defined at 0.0 V, have almost vanished at −1.0 V. The feature at 629 cm^{-1} cannot be assigned to a Fe(III)−O stretching, since this motion appears at wave-

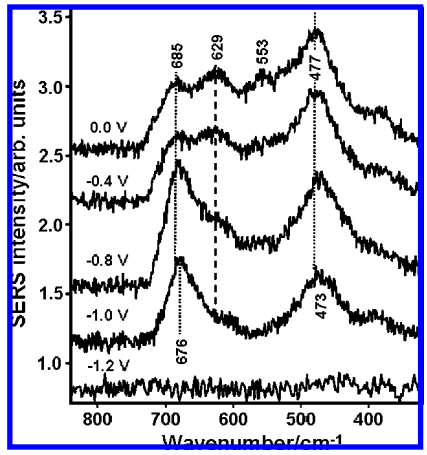

Figure 6. SERS spectra of a $CoFe_2O_4$ thin film deposited on Au at the indicated potentials. The electrolyte solution was a 0.1 mol L^{-1} KCl solution. The spectra were excited at 632.8 nm.

numbers above 660 cm^{-1} for different Fe(III) oxides, hydroxides, or oxihydroxides.[44,45] Therefore, we tentatively assign this feature to a phonon involving the Co−O motion at octahedral sites. Note that the intensity of the phonon at 553 cm^{-1} follows the same dependence on the applied potential as the one at 629 cm^{-1}. Therefore, it may also be assigned to a phonon mode involving a Co−O motion.

The voltammetric behavior of Co hydroxides and oxihydroxides in 6 mol L^{-1} KOH solution was investigated by Elumalai et al.[64] These authors have observed that the CoOOH species reduces to $Co(OH)_2$ at 0.3 V vs Hg/HgO (~0.2 V vs SCE) and that the $Co(OH)_2$ reduces to Co near −1.1 V vs Hg/HgO (~−1.2 V vs SCE). At pH near 7 (the case for the SERS measurements reported here), these Co species would reduce near 0.7 and −0.7 V vs SCE, respectively. Therefore, the presence of Co(III) species on the $CoFe_2O_4$ nanoparticles can be ruled out. Since the features near 629 and 553 cm^{-1} have their intensities decreasing for potentials more negative than −0.4 V, the assignment of these features to Co−O motions seems to be correct. SERS signals at 685 and 477 cm^{-1} are then assigned to phonons involving Fe(III)−O motions. As the potential is made more negative, these features shift to 676 and 473 cm^{-1}, respectively. The feature at 676 cm^{-1} can be assigned to an iron oxide with a structure similar to magnetite, since this value is very close to the one observed in the magnetite obtained after the reduction of maghemite at the same pH.[45] In addition, as observed in the SERS of maghemite, the magnetite signal vanishes for potential more negative than −1.0 V,[45] as is also shown in Figure 6. Note that the signal near 473 cm^{-1} has also vanished at −1.2 V; therefore, we believe that it also involves an Fe(II)−O motion.

3.4. Raman Spectra of Magnetic Fluids. It is very rare to see reports on the Raman spectra of magnetic fluids; that is, from colloidal dispersions of magnetic nanoparticles in a carrier solvent. In this sense, the Raman spectra of the MF, or colloidal dispersions of Fe_3O_4/SO, Fe_3O_4/CO, and $CoFe_2O_4$/SO nanoparticles in cyclohexane are displayed in Figure 7a−c. The Raman signals of the solvent (marked with asterisks in Figure 7) and of the indicated ferrite phonons are well-resolved. Note that the Raman phonons appear at the same wavenumber positions and with the same relative intensities as in Figure 3 for the solid samples. It is then interesting to notice that although the DRIFT spectra (Figure 1) provide more information regarding the fatty acid coordination, the Raman spectra (Figures 3 and 7) probed the density of phonon states in the magnetic nanoparticles. The

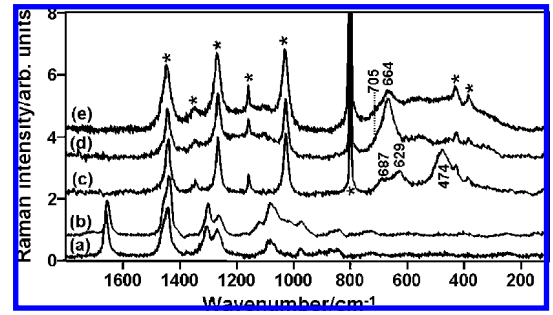

Figure 7. Raman spectra of soybean (a) and castor oil (b) fatty acids and $CoFe_2O_4$/SO (c), Fe_3O_4/CO (d), and Fe_3O_4/SO magnetic fluids in cyclohexane. *, cyclohexane peaks.

Raman spectra of the two fatty acids used in the present work are also displayed in Figure 7a and b to show that in the 100−1700 cm^{-1} spectral region, there is no Raman signal characteristic of the fatty acids in the Raman spectra of the MF of Figure 7c−e. We have observed characteristic signals of adsorbed fatty acids in the CH stretching region, near 2930 and 2860 cm^{-1} (asymmetric and symmetric CH_2 stretching, respectively), only when the Raman spectra of the solid samples were recorded but with a very poor signal-to-noise ratio.

Conclusion

The results presented in this work show that Fe_3O_4 and $CoFe_2O_4$ can be modified by the adsorption of soybean and castor oil fatty acids, leading to the formation of magnetic particles with mean diameters in the range of 10−15 nm. The fatty acid modified magnetic particles can be readily dispersed in nonpolar solvents, forming magnetic fluids. The DRIFT spectra of the modified nanoparticles show that the fatty acids adsorb on the ferrite surface by the interaction of the carboxylate group, forming mono and bidentate structures or even by interaction with the carboxylic group, forming a bridge bidentate quelate. The Raman spectra of the magnetic fluids (modified ferrites dispersed in cyclohexane) are quite similar to those of solid samples except for the solvent Raman signals. Raman signals characteristic of the fatty acid-modified ferrites are observed in the CH stretching region only for the solid samples.

The FTIR and Raman spectra of the nonmodified magnetite particles show that they are partially oxidized, probably by the formation of a nonstoichiometric Fe(III) oxyhydroxide. The FTIR as well as the Raman spectra of the Fe_3O_4 and $CoFe_2O_4$ nanoparticles show a larger number of active phonons than expected for the corresponding bulk crystals. Moreover, IR phonons were observed in the Raman spectra and vice versa which is not predictable for an inverse spinel cubic structure. We interpreted these observations as a quantum size effect. Due to the small size of the particles as compared to the wavelength, there is a breakdown in the momentum conservation rule, and phonons for $k \neq 0$ become active. Finally, the SERS measurements of a $CoFe_2O_4$ thin film on a gold electrode at different applied potentials have shown that the phonons near 680 and 470 cm^{-1} have contributions from Fe(III)−O motions, whereas those observed near 550 and 630 cm^{-1} involve Co−O motions.

Acknowledgment. The authors thank FINATEC, FAPDF, Finep/CTEnerg, CAPES, and CNPq for financial support. G.V.M.J. thanks CAPES; P.C., P.A.Z.S., and J.C.R. thank CNPq for research fellowships. A.G.B. is thankful for research support from NSERC, CFI, and BCKDF.

Supporting Information Available: The fatty acid profile of vegetable oils (soybean and castor oils, Table 1S), the

magnetic fluid experiencing a static magnetic field (Figure 1S), RDX spectra of MFe_2O_4 (M = Fe, Co) nanoparticles (Figure 2S), TEM images magntetite (Figure 3S) and $CoFe_2O_4$ (Figure 4S) nanoparticles, FTIR transmission spectra of the fatty acids (Figure 5S), FTIR curve fitted spectra of the ferrite samples (Figure 6S), Raman curve fitted spectra of the ferrite samples (Figure 7S), and Raman spectra of the modified magnetic particles (solid samples) in the CH stretching region (Figure 8S).This material is available free of charge via the Internet at http://pubs.acs.org.

References and Notes

(1) Bitter, F. *Phys. Rev.* **1932**, *41*, 507–515.
(2) Elmore, W. C. *Phys. Rev.* **1938**, *54*, 309–310.
(3) Papell, S. S. U.S. Patent 3215572, 1965.
(4) Rosensweig, R. E. U.S. Patent 3917538, 1975.
(5) Rosensweig, R. E. *Ferrohydrodynamics*; Cambridge University Press: Cambridge, 1985.
(6) Massart, R. France Patent 7918842, 1979.
(7) Tourinho, F. A.; Franck, R.; Massart, R.; Perzynski, R. *Prog. Colloid Polym. Sci.* **1989**, *79*, 128–134.
(8) Tourinho, F. A.; Franck, R.; Massart, R. *J. Mater. Sci.* **1990**, *25*, 3249–3254.
(9) Laurent, S.; Forge, D.; Port, M.; Roch, A.; Robic, C.; Elst, L. V.; Muller, R. N. *Chem. Rev.* **2008**, *108*, 2064–2110.
(10) Sousa, M. H.; Rubim, J. C.; Sobrinho, P. G.; Tourinho, F. A. *J. Magn. Magn. Mater.* **2001**, *225*, 67–72.
(11) Macaroff, P. P.; Simioni, A. R.; Lacava, Z. G. M.; Lima, E. C. D.; Morais, P. C.; Tedesco, A. C. *J. Appl. Phys.* **2006**, *99*, 08S1021-3.
(12) Jordan, A.; Scholz, R.; Maier-Hauff, K.; van Landeghem, F.; Waldoefner, N.; Teichgraeber, U.; Pinkernelle, J.; Bruhn, H.; Neumann, F.; Thiesen, B.; von Deimling, A.; Felix, R. *J. Neuro-Oncol.* **2006**, *78*, 7–14.
(13) Tadmor, R.; Rosensweig, R. E.; Frey, J.; Klein, J. *Langmuir* **2000**, *16*, 9117–9120.
(14) Rockenberger, J.; Scher, E. C.; Alivisatos, A. P. *J. Am. Chem. Soc.* **1999**, *121*, 11595–11596.
(15) Suslick, K. S.; Fang, M. M.; Hyeon, T. *J. Am. Chem. Soc.* **1996**, *118*, 11960–11961.
(16) Hyeon, T.; Lee, S. S.; Park, J.; Chung, Y.; Bin Na, H. *J. Am. Chem. Soc.* **2001**, *123*, 12798–12801.
(17) Sun, S. H.; Zeng, H.; Robinson, D. B.; Raoux, S.; Rice, P. M.; Wang, S. X.; Li, G. X. *J. Am. Chem. Soc.* **2004**, *126*, 273–279.
(18) Park, J.; An, K. J.; Hwang, Y. S.; Park, J. G.; Noh, H. J.; Kim, J. Y.; Park, J. H.; Hwang, N. M.; Hyeon, T. *Nat. Mater.* **2004**, *3*, 891–895.
(19) Wang, X.; Zhuang, J.; Peng, Q.; Li, Y. *Nature (London)* **2005**, *437*, 121–124.
(20) Wang, Y.; Maksimuk, S.; Shen, R.; Yang, H. *Green Chem.* **2007**, *9*, 1051.
(21) Gasparov, L. V.; Tanner, D. B.; Romero, D. B.; Berger, H.; Margaritondo, G.; Forro, L. *Phys. Rev. B* **2000**, *62*, 7939–7944.
(22) Shemer, G.; Tirosh, E.; Livneh, T.; Markovich, G. *J. Phys. Chem. C* **2007**, *111*, 14334–14338.
(23) Wang, Z. W.; Downs, R. T.; Pischedda, V.; Shetty, R.; Saxena, S. K.; Zha, C. S.; Zhao, Y. S.; Schiferl, D.; Waskowska, A. *Phys. Rev. B* **2003**, *68*, 0941011–6.
(24) Gomes, J. D.; Sousa, M. H.; Tourinho, F. A.; Aquino, R.; da Silva, G. J.; Depeyrot, J.; Dubois, E.; Perzynski, R. *J. Phys. Chem. C* **2008**, *112*, 6220–6227.
(25) White, W. B.; DeAngelis, B. A. *Spectrochim. Acta* **1967**, *23A*, 985–995.
(26) Chamritski, I.; Burns, G. *J. Phys. Chem. B* **2005**, *109*, 4965–4968.
(27) Chourpa, I.; Douziech-Eyrolles, L.; Ngaboni-Okassa, L.; Fouquenet, J. F.; Cohen-Jonathan, S.; Souce, M.; Marchais, H.; Dubois, P. *Analyst* **2005**, *130*, 1395–1403.
(28) Viart, N.; Rebmann, G.; Pourroy, G.; Loison, J. L.; Versini, G.; Huber, F.; Ulhaq-Bouillet, C.; Meny, C.; Panissod, P.; Saviot, L. *Thin Solid Films* **2005**, *471*, 40–47.
(29) Wang, W. H.; Ren, X. *J. Cryst. Growth* **2006**, *289*, 605–608.
(30) Knothe, G. *Energy Fuels* **2008**, *22*, 1358–1364.
(31) Morais, P. C.; Garg, V. K.; Oliveira, A. C.; Silva, L. P.; Azevedo, R. B.; Silva, A. M. L.; Lima, E. C. D. *J. Magn. Magn. Mater.* **2001**, 37–40.
(32) Liu, Y. C.; Wang, C. C.; Tsai, C. E. *Electrochem. Commun.* **2005**, *7*, 1345–1350.
(33) Lee, D. H.; Condrate, R. A.; Lacourse, W. C. *J. Mater. Sci.* **2000**, *35*, 4961–4970.
(34) Soderlind, F.; Pedersen, H.; Petoral, R. M.; Kall, P. O.; Uvdal, K. *J. Colloid Interface Sci.* **2005**, *288*, 140–148.
(35) Egerton, T. A.; Everall, N. J.; Tooley, I. R. *Langmuir* **2005**, *21*, 3172–3178.
(36) Ren, Y.; Kato, T. *Langmuir* **2002**, *18*, 8560–8565.
(37) Kariuki, N. N.; Luo, J.; Hassan, S. A.; Lim, I. I. S.; Wang, L. Y.; Zhong, C. J. *Chem. Mater.* **2006**, *18*, 123–132.
(38) Seo, Y. U.; Lee, S. J.; Kim, K. *J. Phys. Chem. B* **2004**, *108*, 4000–4007.
(39) Nakamoto, K. *Infrared and Raman Spectra of Inorganic and Coordination Compounds*; Wiley: New York, 1986.
(40) Degiorgi, L.; Blattermorke, I.; Wachter, P. *Phys. Rev. B* **1987**, *35*, 5421–5424.
(41) Shebanova, O. N.; Lazor, P. *J. Solid State Chem.* **2003**, *174*, 424–430.
(42) Nasrazadani, S.; Namduri, H. *Spectrochim. Acta B* **2006**, *61*, 565–571.
(43) de Faria, D. L. A.; Silva, S. V.; de Oliveira, M. T. *J. Raman Spectrosc.* **1997**, *28*, 873–878.
(44) Sousa, M. H.; Tourinho, F. A.; Rubim, J. C. *J. Raman Spectrosc.* **2000**, *31*, 185–191.
(45) Jacintho, G. V. M.; Corio, P.; Rubim, J. C. *J. Electroanal. Chem.* **2007**, *603*, 27–34.
(46) Tuinstra, F.; Koenig, J. L. *J. Chem. Phys.* **1970**, *53*, 1126–1130.
(47) Iijima, S.; Yudasaka, M.; Yamada, R.; Bandow, S.; Suenaga, K.; Kokai, F.; Takahashi, K. Chem. Phys. Lett. 1999, *309*.
(48) Handke, B.; Kozłwski, A.; Parliński, K.; Przewoznik, J.; SlJzak, T.; Chumakov, A. I.; Niesen, L.; Kakol, Z.; Korecki, J. *Phys. Rev. B* **2005**, *71*, 1443011–11.
(49) Inaba, N.; Miyajuma, H.; Takahashi, H.; Taketomi, S.; Chikazumi, S. *IEEE Trans. Magn.* **1989**, *25*, 3866–3868.
(50) Muret, P. *Solid State Commun.* **1974**, *14*, 1119–1122.
(51) Tang, J.; Myers, M.; Bosnick, K. A.; Brus, L. E. *J. Phys. Chem. B* **2003**, *107*, 7501–7506.
(52) Gabal, M. A.; Ata-Allah, S. S. *Mater. Chem. Phys.* **2004**, *85*, 104–112.
(53) Zhao, L. J.; Zhang, H. J.; Xing, Y.; Song, S. Y.; Yu, S. Y.; Shi, W. D.; Guo, X. M.; Yang, J. H.; Lei, Y. Q.; Cao, F. *J. Solid State Chem.* **2008**, *181*, 245–252.
(54) Liu, X. M.; Fu, S. Y.; Xiao, H. M.; Huang, C. J. *Phys. B: Condens. Matter* **2005**, *370*, 14–21.
(55) Tirosh, E.; Shemer, G.; Markovich, G. *Chem. Mater.* **2006**, *18*, 465–470.
(56) Calero-DdelC, V. L.; Rinaldi, C. *J. Magn. Magn. Mater.* **2007**, *314*, 60–67.
(57) Soler, M. A. G.; Melo, T. F. O.; da Silva, S. W.; Lima, E. C. D.; Pimenta, A. C. M.; Garg, V. K.; Oliveira, A. C.; Morais, P. C. *J. Magn. Magn. Mater.* **2004**, *272*, 2357–2358.
(58) Yu, T.; Shen, Z. X.; Shi, Y.; Ding, J. *J. Phys.: Condens. Matter* **2002**, *14*, L613–L618.
(59) da Silva, S. W.; Melo, T. F. O.; Soler, M. A. G.; Lima, E. C. D.; da Silva, A. F.; Morais, P. C. *IEE Trans. Magn.* **2003**, *39*, 2645–2647.
(60) Soler, M. A. G.; Lima, E. C. D.; da Silva, S. W.; Melo, T. F. O.; Pimenta, A. C. M.; Sinnecker, J. P.; Azevedo, R. B.; Garg, V. K.; Oliveira, A. C.; Novak, M. A.; Morais, P. C. *Langmuir* **2007**, *23*, 9611–9617.
(61) Ortega, N.; Kumar, A.; Bhattacharya, P.; Majumder, S. B.; Katiyar, R. S. *Phys. Rev. B* **2008**, *77*, 0141111–10.
(62) De Guire, M. R.; O'Handley, R. C.; Kalonji, G. *J. Appl. Phys.* **1989**, *65*, 3167–3172.
(63) Qu, Y.; Yang, H.; Yang, N.; Fan, Y.; Zhu, H.; Zou, G. *Mater. Lett.* **2006**, *60*, 3548–3552.
(64) Elumalai, P.; Vasan, H. N.; Munichandraiah, N. *J. Power Sources* **2001**, *93*, 201–208.

JP9013477